Array Synthesis of Circular Huygens Metasurfaces for Antenna Beam-Shaping

Michela Longhi, *Member, IEEE*, S. Vellucci, *Member, IEEE*, M. Barbuto, *Senior Member, IEEE*, A. Monti, *Senior Member, IEEE*, Z. Hamzavi-Zarghani, L. Stefanini, *Graduate Student Member, IEEE*, D. Ramaccia, *Senior Member, IEEE*, F. Bilotti, *Fellow, IEEE*, and A. Toscano, *Senior Member, IEEE*

***Abstract*—In this contribution, we discuss the modeling of cylindrical Huygens metasurfaces wrapping linear antennas through the array antenna theory. In particular, it is shown that the circular array pattern synthesis can be efficiently exploited to model conformal metasurfaces used for wavefront manipulation in view of beamforming applications. By considering the metasurface unit-cells as the equivalent radiating sources of a circular array, the shape of the emerging radiation pattern is accurately predicted. The proposed approach is validated through several examples where the radiation patterns are modified acting on the excitation phases of the equivalent circular array sources, and are compared with full-wave numerical simulations considering ideal coating metasurfaces designed with conventional techniques. This innovative design strategy allows to further expands the possibility enabled by metasurface coatings in radiation pattern manipulation, potentially improving the functionality of metasurfaces through full control over the radiation characteristics.**

***Index Terms*—Antennas array, beamforming, coating metasurfaces, Huygens metasurfaces (HMSs), metasurfaces.**

I. Introduction

THE current wireless communication scenario of 5G and 6G offers great opportunities for the introduction of innovative communication technologies [1]. Indeed, for overcoming the limitations of 5G networks, it is crucial to turn the wireless environment into an adapted, controlled, sensing, and programmable system [2]. In addition, to guarantee a sufficient signal strength and minimize propagation losses due to the use of mm-Waves, it is necessary to implement a denser base stations coverage. However, this may not always be a feasible or economically viable solution due to the high costs of the acquisition of new sites, rental fees, maintenance, and power supply [3]. Moreover, the massive densification of antennas and the changing operational scenarios required the development of compact add-on solutions for adapting pre-existing antennas [4], [5].

In this complex framework, metasurfaces are expected to play an important role as a key enabling technology of future communication systems [6], [7], [8], and devices with reconfigurable capabilities enabled by metasurface coatings can play a crucial role also for achieving a tunable scattering reduction [9], implementing photonic memories [10], increasing performances of communication systems by implementing both space- and frequency-division multiplexing [11], or designing metasurface-coated devices for energy-efficient and secure 6G communications [12]. Moreover, compared to conventional active beamforming solutions for metasurface-based devices (e.g., [13], [14]), we recently proposed the concept of a single feed beam-scanning wire antenna, based on the use of fully passive Huygens metasurface (HMS) coatings. This solution is able to modify the original omnidirectional radiation pattern of a central linear antenna source acting on the precise control of the amplitude and phase of the output fields. [15], [16]. Indeed, HMSs consist of unit-cells that guarantee the full transmission of the impinging field and full control over its phase through a proper combination of the electric and magnetic dipole moments [17], [18]. In addition, the possibility of properly tailoring the electric and magnetic impedances of an HMS allows for a peculiar unidirectional radiation pattern [19]. Thanks to these exciting properties, in the last decade, HMSs have shown wide possibilities in modifying the electromagnetic wavefront and, among them, the design of phase-gradient metasurfaces for refracting in unconventional ways the incoming field is one of the most discussed [20]. More specifically, in [16], we have shown that thanks to their wavefronts manipulation capability, cylindrical HMS mounted around a wire antenna can transform the omnidirectional pattern into multiple beams pointing toward specific desired directions. Indeed, by properly designing a gradient HMS, it is possible to modify the phase-insertion on the H-plane of the wire antenna. In particular, the division of the HMS in multiple and different cells allows to introduce a variation of phase response modeled through the ray-tracing approach, which is simple to implement and use to obtain the desired pointing directions. However, this approach neglects several complex aspects to achieve fine and precise control over the overall radiation pattern shape and direction. Indeed, this method does not take into account the angular response of the

Manuscript received 20 July 2023; revised 2 September 2023; accepted 7 September 2023. Date of publication 15 September 2023; date of current version 1 November 2023. This work was supported in part by the ATEMA-POR FESR LAZIO 2014/2020—Gruppi di Ricerca 2020, funded by the REGIONE LAZIO Prot. N. A0375-2020-36659 (CUP F89J21021490009); and in part by the MANTLES, funded by the Italian Ministry of University and Research under the PRIN 2017 Program (protocol number 2017BHFZKH). *(Corresponding author: Michela Longhi.)*

Michela Longhi, S. Vellucci, and M. Barbuto are with the Department of Engineering, Niccolò Cusano University, 00166 Rome, Italy (e-mail: michela.longhi@unicusano.it; stefano.vellucci@uniroma3.it; mirko.barbuto@unicusano.it).

A. Monti, Z. Hamzavi-Zarghani, L. Stefanini, D. Ramaccia, F. Bilotti, and A. Toscano are with the Department of Industrial, Electronic and Mechanical Engineering, ROMA TRE University, 00146 Rome, Italy (e-mail: alessio.monti@uniroma3.it; zahra.hamzavizarghani@uniroma3.it; luca.stefanini@uniroma3.it; davide.ramaccia@uniroma3.it; filiberto.bilotti@uniroma3.it; alessandro.toscano@uniroma3.it).

Digital Object Identifier 10.1109/LAWP.2023.3315774

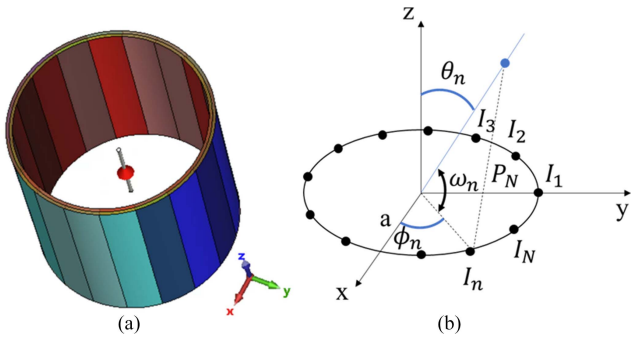

Fig. 1. (a) Schematic of the cylindrical HMS structure placed around the central antenna source. The different colors pictorially represent the phase-gradient introduced by the coat. (b) Geometrical schematic of the 2-D metasurface model based on the circular array theory. The array is composed of *N* elementary radiating sources representing the single unit-cells of the metasurface.

HMS cells as well as the superposition of the different wavefronts in different directions. To overcome these limitations, in this letter, we describe how to improve the model of the proposed system with the use of a circular array synthesis approach. It is also worth noting that, compared to conventional beamforming solutions, cylindrical HMS uses passive metasurfaces that do not require complex, bulky, and power-hungry beamforming networks. Moreover, this solution does not suffer from typical mutual coupling limitations arising between the active elements of the array.

The rest of the letter is organized as follows. Section II describes the design of the HMS using the circular array synthesis. In particular, the working principle for achieving beam manipulation is discussed and the circular array theory is exploited for the modeling of cylindrical HMSs used for coating wire antennas. Then, in Section III, some different beams configurations modeled and designed with the proposed method are presented, and the corresponding results are compared with the ones obtained by full-wave numerical simulations considering ideal coating metasurfaces designed with conventional techniques. Finally, Section IV concludes this letter.

II. Array Theory for the Metasurface Coating Design

In this section, we exploit the antenna array theory for the modeling, design, and performance evaluation of cylindrical HMSs used for coating wire antennas and introducing beamforming functionality. In our recent publication [21], we implemented this kind of HMSs [Fig. 1(a)], designed around a half-wavelength dipole, to introduce a phase-gradient on the azimuth direction and create a modification on the omnidirectional pattern. The proposed HMS consists of anisotropic transition sheets with inhomogeneous unit-cell along the azimuth [22], which allow manipulating the original omnidirectional pattern of the antenna on the *H*-plane direction. Indeed, with this structure, a distributed phase-insertion on the *xy*-plane is introduced [21], leading to a focusing effect and beamforming capabilities on the azimuth plane. In particular, to achieve beamforming functionalities, the HMS should tailor its phase-insertion by transforming the cylindrical wavefront on the horizontal plane into planar wavefronts. The number of new radiation beams is regulated by the spatial periodicity of the phase-insertion function. In [21], the phase-insertion function was evaluated through a ray-tracing approach aiming at defining the phase insertion introduced by the HMS unit-cells and implemented through the surface impedance modulation.

Albeit the efficient beamforming capabilities and the physical working principles of this design approach were demonstrated, some limitations in the radiation pattern design were present, such as the inability to predict the final directivity values of the radiating beams, the sidelobe levels, and the nulls positioning. These limitations can be overcome by modeling the HMS structure as a circular antenna array, whose geometrical representation is shown in Fig. 1(b). In this model, we assume that each cell of the HMS is represented by an antenna element. In this way, we can describe the behavior of the cylindrical HMS using a circular array, consisting of *N* isotropic antenna elements placed on a circle of radius *a* in the *xy*-plane.

The total normalized field radiated by the array is given by

$$E_n(r,\theta,\phi) = \sum_{n=1}^{N} a_n \, e^{-jkP_n}/P_n \tag{1}$$

where k is the wave number, a_n is the excitation coefficient of the nth antenna element, and P_n is the distance of the nth element from the observation point. When considering the far-field approximation $P_n = (r^2 + a^2 - 2ar\cos\omega_n)^{1/2}$, hence, (1) can be specified for the geometry under consideration as

$$E_n(r,\theta,\phi) = \frac{e^{-jkr}}{r} \sum_{n=1}^{N} a_n e^{jka\,\sin\theta\,\cos(\phi-\phi_n)} \tag{2}$$

where ϕ_n is the angular position of the nth radiator on xy-plane, θ represents the elevation angle from the positive z-axis, ϕ is the azimuth angle from the positive x-axis, and where the excitation coefficient of the nth antenna element can be rewritten as $a_n = I_n \, e^{+j\alpha_n}$, with I_n and α_n the excitation amplitude and phase, respectively.

From (2), we can observe that the expression of the total electric field of the array is defined by the field of a single radiating element multiplied by the array factor [23]

$$\mathrm{AF}(\theta,\phi) = \sum_{n=1}^{N} I_n e^{j[ka\,\sin\theta\cos(\phi-\phi_n)+\alpha_n]} \tag{3}$$

reducing (2) to

$$E_n(r,\theta,\phi) = \frac{e^{-jkr}}{r}\,\mathrm{AF}(\theta,\phi)\,. \tag{4}$$

For pointing the main beam toward (θ_0, ϕ_0), the excitation phases in (3) must be chosen as [23]

$$\alpha_n = -ka\,\sin\theta_0\,\cos(\phi_0 - \phi_n)\,. \tag{5}$$

In our case, since we focus our attention on steering the radiation pattern on the *H*-plane of the antenna (i.e., the *xy*-plane), θ is assumed to be 90°.

It is worth noticing that, to correctly model the HMS coating, the number of radiating elements should be the same as the HMS cells and the radius a should be equal to the HMS radius. More importantly, the Huygens cells composing the metasurface are characterized by a directive element pattern that must be judiciously taken into account for the proper evaluation of the

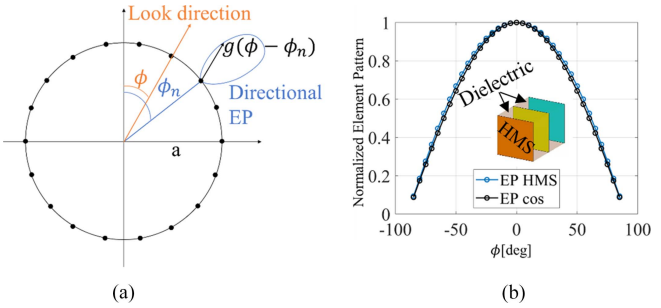

Fig. 2. (a) Pictorial representation of the element pattern in the circular array schematic when compared to the main look direction of the array. (b) HMS unit-cell schematic composed by three metasurface layers and two thin dielectric substrates, and its radiating pattern compared to the cosine function.

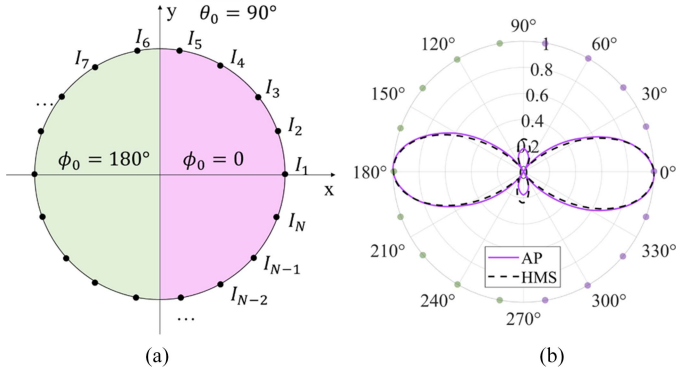

Fig. 3. (a) Schematic of the circular array when it is divided into two semicircular sectors with the main lobes radiating toward $\phi_0 = 0°$ and $\phi_0 = 180°$. (b) Normalized directivity pattern of the proposed configuration evaluated through the antenna array theory and compared with the response of an equivalent HMS coat designed through the ray-tracing approach. Colored dots represent the geometric position of the antennas in the array.

overall array pattern. Namely, Huygens cells are characterized by an element pattern pointing at the boresight with ideally zero backscattering. In addition, in a circular array configuration, the element pattern plays an important role in the total array pattern since each element is facing a different direction depending on the position of the element itself. In other terms, the element pattern expression has a different value in each summand of (4). This concept is graphically illustrated in Fig. 2(a), where the *n*th element of the array is schematically shown with its element pattern. As can be observed, due to the curved geometry of the array, the single Huygens radiating element points toward a ϕ_n direction, which could be different from the pointing direction of the array. In addition, to define the element pattern, we have to consider that the HMS cells exhibit a nonconstant angular response in the forward direction, as shown in Fig. 2(b) (blue line). To properly characterize the element pattern of the single Huygens cell [Fig. 2(b)], full-wave simulations when considering a stacked configuration of impedance sheets typically used to properly collocate the electric and magnetic dipole moments ensuring forward propagation are implemented. Indeed, this configuration is the one considered in [16] and used as a reference. Considering a phase-insertion profile on the azimuthal plane, θ is assumed to be 90° and by imposing periodic boundary conditions and considering Floquet modes excitation, the element pattern from the antenna source can be extracted. As can be appreciated in Fig. 2(b), the cell element pattern well fits a cosine function and can be thus defined as

$$g_n(\phi) = \begin{cases} \cos(\phi - \phi_n) & -90° < \phi - \phi_n < 90° \\ 0 & \text{otherwise} \end{cases}. \quad (6)$$

As expected, the extracted Huygens cell scattering pattern is consistent with the results discussed in [24]. Please note that (6) assumes constant behavior of the element pattern on the θ plane. Finally, once derived the expressions for the cell element pattern and the array factor, the overall array pattern is expressed as

$$\text{AP}(\phi) = \sum_{n=1}^{N} I_n \, e^{j[ka \, \sin\theta \cos(\phi-\phi_n)+\alpha_n]} g_n(\phi) \quad (7)$$

and the directivity of the circular array $D(\theta, \phi)$ can be thus evaluated as

$$D(\theta,\phi) = \frac{4\pi |AP_{\max}|^2}{\int_0^{2\pi}\int_0^{\pi} |AP(\theta,\phi)|^2 d\theta d\phi}. \quad (8)$$

It is worth noting that for the comparison with our three-dimensional scenario, (8) returns valid results just for $\theta = 90°$ since we assumed the element pattern to be a function just of the azimuth angle. Still, (8) would return valuable results for each elevation plane when including in (6) the dependence of the single element response also on the elevation angle.

III. Beamforming Configurations

In this section, we validate the presented antenna array model for a circular HMS, discussing three different array configurations.

We compare the analytically derived results in terms of expected radiation patterns with the ones coming from the synthesis of the HMS through the ray-tracing approach presented in [16]. In the latter, the unit-cells are implemented in a full-wave EM simulation tool as subwavelength constituents of the cylindrical HMS coat. Hereinafter, without losing generality, the case of a coating metasurface characterized by a radius $a = \lambda_0/2$ and operating frequency $f_0 = 3$ GHz is considered.

A. Two Sectors

As a first example, let us consider the case of an HMS used to produce two symmetric beams radiating at opposite sides. In order to create two symmetric beams along the *x*-axis, in (3), θ_0 is selected as 90° and ϕ_0 as 0° and 180° [Fig. 3(a)]. Hence, the array is divided into two semicircular sectors (i.e., $M = 2$) and each sector is composed of $N/2 = 9$ elements as shown in Fig. 3(a). In other terms, we are considering the case of an HMS consisting of 18 unit-cells. Once the number of main beams and their pointing direction is fixed, (5) is used to derive the values of the excitation phases, while equal excitation amplitudes are assumed.

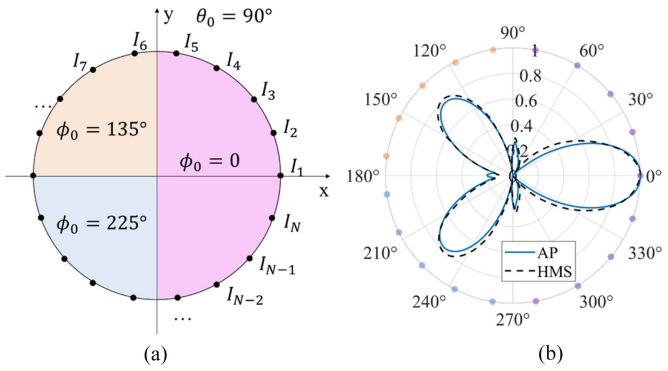

Fig. 4. (a) General schematic of the circular array when it is divided into three sectors with the main lobes radiating toward $\phi_0 = 0°$, $\phi_0 = 135°$, and $\phi_0 = 225°$. (b) Normalized directivity pattern of the $N = 19$ configuration evaluated through the antenna array theory and compared with the response of an equivalent HMS coat designed through the ray-tracing approach.

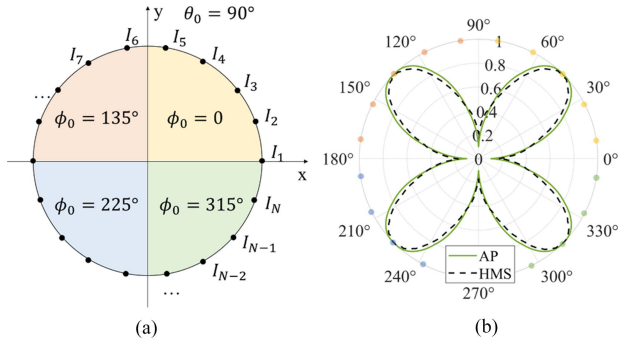

Fig. 5. (a) General schematic of the circular array when it is split in two sectors with the main lobes radiating toward $\phi_0 = 0°$, $\phi_0 = 135°$, $\phi_0 = 225°$, and $\phi_0 = 315°$. (b) Normalized directivity pattern of the proposed $N = 20$ configuration evaluated through the antenna array theory and compared with the response of an equivalent HMS coat designed through the ray-tracing approach.

In Fig. 3(b), the normalized directivity polar pattern of the array configuration (violet line) is compared to the radiation pattern coming from the design of an HMS structure obtained with the ray-tracing approach (black dashed line). A very good matching between the two curves can be observed. The array model accurately predicts the shape of the radiation pattern, the beamwidth, and the sidelobe levels. Moreover, through (8), it is possible to calculate the maximum directivity value which is 6.88 dB. As expected, this is a higher value compared to the maximum value returned from the full-wave results (6.03 dB) since in the latter a realistic HMS configuration is considered. Remarkably, (8) gives an indication of the maximum directivity values that a realistic HMS setup can achieve, expanding the antenna designer possibilities.

B. Three Sectors

Here, we want to evaluate a more complex case to demonstrate the versatility of our approach in accurately modeling the beamforming functionality of HMS coatings. In particular, we consider a three-beam HMS coated linear antenna with $N = 19$ (the number of elements was increased compared to the previous case to ensure an integer number of elements per sector), in which half of the metasurface is pointing toward $\phi_0 = 0°$ and the second half has two main directions, respectively, to 135° and 225°.

The full-wave numerical results of the designed HMS structure compared to the array pattern obtained using the array synthesis approach are reported in Fig. 4(b). Here, once again, the excitation phases of the circular array are derived through (5), while the realistic HMS is designed through the ray-tracing approach. It can be observed a very good agreement between the curves, although a slight deviation of the secondary beams from the full-wave results is reported, mostly due to the mutual coupling between the realistic cells. Moreover, in this scenario, the maximum directivity value analytically evaluated is 6.72 dB, while the directivity value of the secondary lobes points toward $\phi_0 = 135°/225°$ is 5.89 dB. We remark that with the approach proposed in [16], it was not possible to accurately predict the directivity values obtained, as well as the magnitude and pointing directions of the side lobes.

C. Four Sectors

Finally, we report the scenario of an HMS structure able to shape the original omnidirectional pattern of the central antenna element in four different beams. The case of an HMS implemented through 20 unit-cells elements is considered while the pointing direction of the beams are $\phi_0 = 45°; 135°; 225°; 315°$, following the design schematic reported in Fig. 5(a). As can be appreciated from the polar plots in Fig. 5(b), also in this scenario, the radiation pattern is accurately predicted by the antenna array model. Namely, the four radiation beams are identified (with an expected maximum directivity value of 5.55 dB). We remark here that this array model allows simplifying the design of cylindrical HMSs excited by wire antennas and, compared to a ray-tracing approach, provides more information about the overall radiation pattern, such as the maximum directivity, the beamwidth of the main lobes, or the magnitude and pointing directions of the side lobes. In addition, it could be exploited to apply the well-established array synthesis algorithms to the design of HMSs, allowing further tuning capabilities.

IV. Conclusion

In this letter, we have presented an antenna array model for a circular HMS used for introducing beamforming functionalities in linear antennas. Through a rigorous model of the single HMS unit-cells acting as the radiating elements of an equivalent circular array, the excitation phases are analytically derived, which correspond to the phase-insertion values to be introduced by the HMS cells once fixed the desired pointing direction of the radiating beams. Moreover, by exploiting the antenna array theory, the beams' shape and the directivity values are predicted. As a result, we are able not only to design the HMS for specific pointing directions but also to predict, with good accuracy, the beamwidth of the main beams and the side lobes of the overall radiation pattern. The presented model allows further expand the possibility enabled by HMS coatings in manipulating the radiation properties of wire antennas, offering the possibility for a complete synthesis of the radiation pattern. Moreover, it allows for the engineering of the radiation characteristics through the conventional algorithms for array synthesis, an application that may find particular interest in the design of reconfigurable antennas for next-generation communications.

REFERENCES

[1] W. Saad, M. Bennis, and M. Chen, "A vision of 6G wireless systems: Applications, trends, technologies, and open research problems," *IEEE Netw.*, vol. 34, no. 3, pp. 134–142, May/Jun. 2020.

[2] M. F. Yang, D. Erricolo, and A. Massa, "Special issue on smart electromagnetic environment," *IEEE Trans. Antennas Propag.*, vol. 69, no. 3, pp. 1838–1838, Mar. 2021.

[3] R. Flamini et al., "Towards a heterogeneous smart EM environment for millimeter-wave communications: An industrial viewpoint," *IEEE Trans. Antennas Propag.*, vol. 70, no. 10, pp. 8898–8910, Oct. 2022.

[4] S. Vellucci, A. Monti, M. Barbuto, M. Longhi, A. Toscano, and F. Bilotti, "Metasurface coatings enabling scattering, frequency, and radiation tunability for next-generation antenna systems," in *Proc. Microw. Mediterranean Symp.*, 2022, pp. 1–5.

[5] S. Vellucci et al., "Multi-layered coating metasurfaces enabling frequency reconfigurability in wire antenna," *IEEE Open J. Antennas Propag.*, vol. 3, pp. 206–216, 2022.

[6] M. Barbuto et al., "Metasurfaces 3.0: A new paradigm for enabling smart electromagnetic environments," *IEEE Trans. Antennas Propag.*, vol. 70, no. 10, pp. 8883–8897, Oct. 2022.

[7] E. Martini and S. Maci, "Theory, analysis, and design of metasurfaces for smart radio environments," *Proc. IEEE*, vol. 110, no. 9, pp. 1227–1243, Sep. 2022.

[8] G. Oliveri, F. Zardi, P. Rocca, M. Salucci, and A. Massa, "Building a smart EM environment-AI-enhanced aperiodic micro-scale design of passive EM skins," *IEEE Trans. Antennas Propag.*, vol. 70, no. 10, pp. 8757–8770, Oct. 2022.

[9] X.-Y. Luo et al., "Active cylindrical metasurface with spatial reconfigurability for tunable backward scattering reduction," *IEEE Trans. Antennas Propag.*, vol. 69, no. 6, pp. 3332–3340, Jun. 2021.

[10] A. Abrashuly and C. Valagiannopoulos, "Photonic memory with nonlinear plasmonic nanotubes," *Appl. Phys. Lett. Mater.*, vol. 9, no. 10, 2021, Art. no. 101111.

[11] L. Zhang et al., "A wireless communication scheme based on space-and frequency-division multiplexing using digital metasurfaces," *Nature Electron.*, vol. 4, pp. 218–227, 2021.

[12] T. A. Tsiftsis, C. Valagiannopoulos, H. Liu, A.-A. A. Boulogeorgos, and N. I. Miridakis, "Metasurface-coated devices: A new paradigm for energy-efficient and secure 6G communications," *IEEE Veh. Technol. Mag.*, vol. 17, no. 1, pp. 27–36, Mar. 2022.

[13] M. Selvanayagam and G. V. Eleftheriades, "Experimental demonstration of active electromagnetic cloaking," *Phys. Rev. X*, vol. 3, no. 4, 2013, Art. no. 041011.

[14] M. Boyarsky et al., "Electronically steered metasurface antenna," *Sci. Rep.*, vol. 11, no. 1, 2021, Art. no. 4693.

[15] S. Vellucci, M. Longhi, A. Monti, M. Barbuto, A. Toscano, and F. Bilotti, "Antenna pattern shaping through functionalized metasurface coatings," in *Proc. 16th Int. Congr. Artif. Mater. Novel Wave Phenomena (Metamaterials)*, 2022, pp. 466–468.

[16] S. Vellucci, M. Longhi, A. Monti, M. Barbuto, A. Toscano, and F. Bilotti, "Phase-gradient Huygens metasurface coatings for dynamic beamforming in linear antennas," *IEEE Trans. Antennas Propag.*, to be published, doi: 10.1109/TAP.2023.3297193.

[17] C. Pfeiffer and A. Grbic, "Metamaterial Huygens' surfaces: Tailoring wave fronts with reflectionless sheets," *Phys. Rev. Lett.*, vol. 110, 2013, Art. no. 197401.

[18] M. Selvanayagam and G. V. Eleftheriades, "Discontinuous electromagnetic fields using orthogonal electric and magnetic currents for wavefront manipulation," *Opt. Exp.*, vol. 21, no. 12, pp. 14409–14429, 2013.

[19] V. S. Asadchy, M. Albooyeh, S. N. Tcvetkova, A. Díaz-Rubio, Y. Ra'di, and S. A. Tretyakov, "Perfect control of reflection and refraction using spatially dispersive metasurfaces," *Phys. Rev. B*, vol. 94, no. 7, 2016, Art. no. 075142.

[20] M. Chen, E. Abdo-Sánchez, A. Epstein, and G. V. Eleftheriades, "Theory, design, and experimental verification of a reflectionless bianisotropic Huygens' metasurface for wide-angle refraction," *Phys. Rev. B*, vol. 97, 2018, Art. no. 125433.

[21] A. Monti et al., "Quadratic-gradient metasurface-dome for wide-angle beam-steering phased array with reduced gain loss at broadside," *IEEE Trans. Antennas Propag.*, vol. 71, no. 2, pp. 2022–2027, Feb. 2023.

[22] A. Monti et al., "Optimal design of Huygens metasurfaces for oblique incidence through a microwave network approach," in *Proc. Microw. Mediterranean Symp.*, 2022, pp. 1–4.

[23] C. A. Balanis, *Antenna Theory: Analysis and Design*. Hoboken, NJ, USA: Wiley, 2015.

[24] M. I. Abdelrahman et al., "Experimental demonstration of spectrally broadband Huygens sources using low-index spheres," *Appl. Phys. Lett. Photon.*, vol. 4, 2019, Art. no. 020802.